Title
STRUCTURE AND PROPERTIES OF THERMAL-MECHANICALLY TREATED 304 STAINLESS STEEL

Authors
Mangonon, P.L.
Thomas, G.

Publication Date
1969-06-01

Submitted to Transactions of the AIME

UCRL-18869
Preprint

cy. 2
(cy. 2 msg)

STRUCTURE AND PROPERTIES OF THERMAL-MECHANICALLY TREATED 304 STAINLESS STEEL

P. L. Mangonon, Jr. and G. Thomas

June 1969

AEC Contract No. W-7405-eng-48

LAWRENCE RADIATION LABORATORY
UNIVERSITY of CALIFORNIA BERKELEY

(cy 2 msg) cy 3

UCRL-18869

DISCLAIMER

DISCLAIMER

UCRL-18869

STRUCTURE AND PROPERTIES OF THERMAL-MECHANICALLY TREATED 304 STAINLESS STEEL

by

P. L. Mangonon, Jr.* and G. Thomas

Inorganic Materials Research Division, Lawrence Radiation Laboratory, Department of Materials Science and Engineering, College of Engineering, University of California, Berkeley, California

ABSTRACT

Mechanical and thermal-mechanical treatments of 304 stainless steel enables yield strengths of over 200,000 psi to be obtained with elongations better than 10%. Electron microscopy. X-ray, and magnetic techniques show that during deformation, strain induced $\gamma \rightarrow \varepsilon \rightarrow \alpha$ transformation occurs with further thermal nucleation of α achieved by aging up to 400°C. The yield strength is linearly proportional to the amount of α irrespective of the treatment used to form α. The yield strength is given by $\sigma y = 255\ f + 48{,}650$ psi, where f is the volume fraction of martensite. Softening occurs by aging at 500°C and above due to a decrease in % α, which may occur by renucleation of γ. The amount of ε decreases as α increases, by reversion $\varepsilon \rightarrow \gamma$.

The system is thus an unusual form of composite strengthening; hard martensite particles are formed within the austenite, and the % α (and thereby the mechanical properties), can be controlled by the mechanical/thermal-mechanical processing.

---

*Present address: Inland Steel Research Laboratories
East Chicago, Indiana 46312

I. INTRODUCTION

The stability of austenite against the martensitic transformation is usually measured by the M_s and M_d temperatures. The M_s signifies the temperature at which the austenite starts to transform spontaneously to martensite on cooling, while M_d is the temperature above which deformation stresses cannot initiate the transformation. In the case of 304 stainless steels, the authors[1] have shown that the transformation sequence is $\gamma \rightarrow \varepsilon \rightarrow \alpha$ with $M_s^{(\alpha)} < 4°K$ and $M_d^{(\alpha)} \sim 293°K$. In fact α is only observed after mechanical or thermal-mechanical processing. It is thus possible to induce the martensitic transformation in these alloys by sub-zero deformation ("Zerolling"), and this is known to considerably increase the yield and tensile strengths.[1-10] Further significant increases in these properties have been achieved by stress relief treatment between 225° - 425°C,[2,8,9] or by aging.[6,7] An optimum aging temperature of 400°C was established by Chukhleb and Martynov[8] where the maximum increase in properties was observed. The increase in properties at a certain aging temperature depended both on the time of aging and the amount of prior sub-zero deformation. Most of the increase occurred during the first hour of aging followed by a very slight increase but no apparent softening effect occurred even after 120 hours, which makes the phenomenon quite different from that of precipitation hardening. With the increase in mechanical properties, the magnetic susceptibility also increases.

The only attempt made so far to explain the strengthening observed on stress-relief aging is that due to Chukhleb and Martynov.[8] They proposed that precipitation of carbides in the retained austenite occurs followed by nucleation of the α-phase around the carbides. Additional strengthening was

also presumed to result from precipitation of carbides in the stress-induced α-phase. Aside from magnetic susceptibility measurements, no other structural information was obtained.

The purpose of this part of the investigation which is related to Part One [1] was to correlate the properties at room temperature of deformed 304 stainless steels, before and after aging treatments, with quantitative structural information such as volume fractions of γ, α and ε phases obtained from magnetic measurements, and X-ray, light and transmission electron metallography techniques, in order to ascertain the principal mechanism of strengthening.

II. EXPERIMENTAL

The mechanical deformation was carried out in tension at liquid nitrogen using a special arrangement for the Instron machine, whereby the specimen can be completely immersed in the coolant. Some specimens were also rolled at -196°C. Aging was done for one and one-half hour periods at room temperature to 500°C.

Further thermal-mechanical treatment by rolling was also conducted after the first aging treatment to see if further strengthening were possible. The changes in structure were investigated by using the magnetic, X-ray and transmission electron metallography techniques which are described in detail elsewhere [11] (see also Ref. 1).

III. RESULTS

A. Mechanical Properties:

The tensile properties at room temperature after the appropriate thermal

mechanical treatment are shown in Figs. 1-3 and in Table I. Figure 1 shows the yield strength at room temperature after aging at 100°C, 200°C, 400°C, and 500°C subsequent to varying amounts of tensile deformation at -196°C. The yield strengths of the annealed sample at room temperature and at -196°C are also shown for comparison purposes. The points corresponding to aging at room temperature represent properties of as-deformed samples at -196°C brought up to the testing temperature. It is observed that the yield strength was significantly increased from 43,500 psi at the annealed condition to 215,000 psi after 24% tensile strain at -196°C. On the other hand, the effect of temperature on the yield strength in the annealed condition was very small as seen by comparing the yield strength obtained at -196°C to that at room temperature. The latter behavior is understandable if the alloy remains single phase fcc (for example Ref. 12). The ultimate tensile strengths (UTS) Fig. 2, were also considerably increased by deformation at -196°C. In contrast to the yield strength, the UTS in the annealed condition was very temperature-dependent which is again typical of fcc materials, although, as will be shown later, the major factor to be considered is transformation to α-martensite. As expected, the increase in the yield and tensile strengths brought about a decrease in elongation, as illustrated in Fig. 3.

The increase in the yield strength was most marked on aging when the prior deformation was 15% or more. Overaging occurred above 400°C (Figs. 1 and 2).

The ductilities (% elongation) of the samples are shown in Fig. 3. Again for comparison purposes, the elongations of the annealed sample when

tested at room temperature and at -196°C are also shown. It is seen that the maximum tensile strain before fracture that can be imparted to this steel at -196°C is about 30%. As shown by the curves corresponding to the 4% and 15% strained samples, the elongation after aging was at least as high or slightly higher than the as-deformed value. What is significant is the fact that for the 15% strained sample, this increase in ductility is concurrent with increases in yield and tensile strengths. The data points with asterisk marks represent specimens that broke outside the 2" gage marks which explains why the curve for the 10% strained sample is below that for the 15%. For the 20% strained samples, two samples broke within the gage length and the elongations were 11.8% and 11% (see Table I). These treatments thus appear to be promising for obtaining yield strengths in excess of 200,000 psi with at least 10% elongation.

The effects of further thermal-mechanical treatment after the first stress-relief treatment are shown in Table II. Comparing the results in Tables I and II with respect to 20% deformation, it is seen that almost identical properties were obtained whether the deformation was in tension or compression.

Comparing samples A21 and A22, (Table II) it is seen that deformation at 400°C, instead of just aging, resulted in higher yield strengths. The effect of temperature of deformation can be seen by comparing samples A22, A31, and A41. It should also be noted that A31 and A41 were rolled at room temperature and -196°C, respectively, after the first stress-relief treatment at 400°C. The results illustrate that further deformation does not affect the yield strength very much. However, further aging at 400°C resulted

in a considerable increase in strength (samples A32 and A42) and it is seen that the response of A41 (deformed at -196°C) is significantly higher than A31 (deformed at 20°C). The resulting yield strengths of A32 and A42 are higher than A22. The stress-strain curves of the samples aged at 400°C invariably were of Type-III,[13] characterized by no work hardening and sudden drop in load as soon as yielding has occurred.

The changes in properties resulting from the thermal-mechanical treatments were associated with transformation of the austenite to α (martensite) since the specimens became magnetic. Quantitative estimates of the volume fraction of α were obtained both by magnetic and X-ray techniques. Appendix 1 describes how the volume fraction of α is determined from the magnetic measurements.

B. Magnetic Properties:

The intrinsic saturation magnetization, B_s, is structure-insensitive[14] and depends only on the quantity of ferromagnetic phase. Of the three phases, γ, ε, and α, that can co-exist in 304 stainless steel, α is the only ferromagnetic phase. The results of the magnetization measurements are tabulated in Table III and shown in Figs. 4 and 5. Figure 4 illustrates the increase in magnetization, B_s as a function of deformation at -196°C showing that stress-induced transformation of γ to α occurs. Figure 5 shows the change in magnetization, ΔB_s, from the magnetization, B_s, of the as-deformed sample after aging at 100°C, 200°C, 400°C, and 500°C. The peaks at 400°C correspond to a maximum in %α which correlates with the maxima in yield strengths (Fig. 1).

C. X-ray Results:

The X-ray diffractometer traces obtained after a sample was 10% tensile

deformed (-196°C) are shown in Fig. 6. The appearance of the $(10.1)_\varepsilon$ and $(100)_\varepsilon$ peaks in the as-deformed condition (Fig. 6a) indicated the existence of the ε- hcp phase. The relative 2θ values of these peaks with respect to the $(200)_\gamma$, $(111)_\gamma$, and $(110)_\alpha$ using CuKα radiation with a (200) LiF diffracted beam monochromator are shown in the figure. The amount of each phase present in the mixture was determined by comparing the relative integrated intensities of the $(200)_\gamma$, $(10.1)_\varepsilon$, and $(200)_\alpha$ peaks for each amount of tensile strain and the results are shown in Fig. 7. Figure 7 shows that the amount of α steadily increased as the tensile strain increased while the amount of ε maximises at about 5% strain and steadily decreased thereafter. These results agree with published data.[15,16] Figure 7 indicates that the %γ decreased linearly with strain and predicts that 100% α would be present after about 35% strain.

Figure 6 indicates that the ε - hcp phase shown by the $(10.1)_\varepsilon$ peak started to disappear upon aging at 200°C. Samples aged at 100°C did not seem to affect the relative integrated intensity of the $(10.1)_\varepsilon$ peak. These observations suggest that ε starts to revert to γ at about 200°C which was also indicated by Reed.[17] The increase in %γ is indicated by the intensities of the $(200)_\gamma$ and $(111)_\gamma$ peaks before and after aging. After aging at 400°C, the ε disappeared completely, at least to the extent that it can no longer be detected by X-rays. A detectable increase in the amount of α was also observed after aging at 400°C and this is shown in Fig. 8 by the increase in the relative integrated intensity of the $(200)_\alpha$ peak.

D. Transmission Electron Microscopy:

The results of transmission electron microscopy are summarized as follows:

(1) α was nucleated subsequent to formation of ε by deformation at

low temperatures. Thus, in 304 the transformation proceeds $\gamma \rightarrow \varepsilon \rightarrow \alpha$ and not $\gamma \rightarrow \alpha$ ($\rightarrow\varepsilon$). These results have been discussed in detail in the first paper.[1]

(2) The decrease in % ε with aging (Fig. 7) occurred by reversion to γ (by unfaulting) and as a result of growth of α which consumes the neighboring ε phase (Ref. 1) as shown in Figs. 9,10. Observations of dislocation nodes showed that they decreased in radius and became almost irresolvable after 400°C aging.[11] This indicates an increase in stacking fault energy with increasing temperature, i.e., a decrease in stability of the hcp ε phase. The transformation $\gamma \rightleftarrows \varepsilon$ is thus reversible and can be understood on the basis of dissociation of dislocations into partials ($\gamma \rightarrow \varepsilon$) and recombination of partials into whole dislocations ($\varepsilon \rightarrow \gamma$). Such events have been observed directly in Al-Ag alloys.[18]

(3) The increase in amount of α upon aging up to 400°C was found to be due to nucleation of new particles of α rather than growth of existing α particles. The thermally nucleated α is lenticular in appearance similar to martensite in low alloy steels (compare Figs. 10, 11).

(4) Overaging above 400°C is associated with a decrease in % α, i.e., α transforms back to γ. This transformation may occur by renucleation of γ within α rather than by simple disolution of α as indicated in Fig. 12.

(5) The transformed α is representative of dislocated martensite; twinned martensite was not observed.[19]

IV. DISCUSSION OF RESULTS

A. Strengthening Mechanism

Figures 1 and 2 show that considerable increases in both the yield

and tensile strengths is attainable with the 304 stainless steel by mechanical and thermal-mechanical treatments (Tables I and II). The increase in yield strength may be correlated with the increase in dislocation density within the matrix as a result of work hardening during deformation, and precipitation of α during deformation and subsequent aging (Figs. 9-12). These methods have also been utilized to improve the toughness of high strength steels.[20]

Since the carbon content is low, carbide formation within α cannot play an important role in strengthening. Some carbides are visible in the strain induced α, but not in the thermally nucleated α (Figs. 10-12). However, when the yield strengths are plotted against % α Fig. 13, it can be seen that a linear relation is obtained. A regression analysis of the data gives σ_y (psi) = 48,650 + 255 f (where f is equal to the volume fraction of α).

There are two possible interpretations of this result viz a) dispersion strengthening or b) composite strengthening. In dispersion strengthening the particles of α in the γ matrix can be considered to be the hard phase due to work hardening as a result of transformation strains.[19] The yield strength would then be expected to depend on particle size and spacing[21] by the Orowan criterion, similar to systems such as TD nickel.[22,23] The volume fraction $f = N\bar{d} = \bar{d}/\bar{\lambda}$, where N is the number of particles per unit length of dislocation line, $\bar{\lambda}$ is the mean particle spacing and $\bar{d}$ the average diameter. Hence, $\sigma_y \propto f(\alpha) \simeq (\bar{d}/\bar{\lambda})$. To explain the strength $\bar{\lambda} \sim$ 100Å-300Å. However the micrographic evidence, e.g., Fig. 10 where $\bar{\lambda} \gtrsim$ 500Å, and the fact that the yield strength depends not on morphology of α but only on the amount of α (Figs. 10, 11, 13) irrespectively of how the α has been formed, suggests that the system is more aptly described as a composite. Figure 13

is remarkably similar to data obtained for fiber reinforced metals.[24] The yield strength $\sigma_y = 255f + 48.65$ (Fig. 13) may thus be written as a simple law of mixtures[25] $\sigma_y = \sigma^{\alpha} f(\alpha) + \{1 - f(\alpha)\} \sigma^{\gamma}$ where $f(\alpha)$ = volume fraction of α i.e., $\sigma_y = f(\alpha)[\sigma^{\alpha} - \sigma^{\gamma}] + \sigma^{\gamma}$ where $[\sigma^{\alpha} - \sigma^{\gamma}] = 255{,}000$ psi and $\sigma^{\gamma} = 48{,}650$ psi (Fig. 13).

Actually the above equation should probably be modified to include parameters related to the strengthening capacities of the α and γ phases e.g., precipitation hardening, work hardening etc., since the treatments are complex. Thus the magnitude and/or slope of the curve in Fig. 13 may be changed by changing composition (e.g. increasing % carbon) and by further variations in thermal-mechanical treatment. Such effects are being investigated.

Analysis of the true-stress, true-strain relationships at room temperature showed that the work hardening rate is proportional to the square root of the volume fraction of martensite. Although this result may be questionable due to the fact that decomposition to martensite may also occur during testing, it is nevertheless consistent with both the dispersion and composite strengthening models.

B. Martensite Nucleation

It is interesting to comment on the possible ways that the amount of α can increase upon aging. One is that the stress-induced α simply grows. If this were the case, one would expect the boundaries of the "old" α crystals to expand and whatever "new" α comes out, this must have the same orientation as the "old" crystals. However this was not observed as demonstrated by dark field analysis (Fig. 10). Another possibility is that which was envisaged by Chukhleb and Martynov[8] where carbides precipitate out from the

austenite, and the "new" α crystals then form, around the carbides i.e., a nucleation and growth process. This mechanism can also be ruled out on the basis of the transmission electron micrographs (Figs. 10,11). The α particles formed by aging had entirely different orientations from those formed only by deformation; also no precipitation of carbides was observed within them. Furthermore, the new α crystals had a lenticular appearance (Fig. 11) resembling that of martensites in Fe-C and Fe-Ni-C steels and different from the lath-like appearance[1] of the stress-induced α. It is probable therefore that these α crystals formed martensitically by thermal nucleation.[26] This is the first direct evidence, as far as the authors know, of martensites being formed during stress-relief treatment, i.e., on raising the temperature. Such an increase in martensite content had also been monitored magnetically by Kurdjumov, et al.[27] during up-quenching from -196°C to 0°C.

SUMMARY AND CONCLUSIONS

Mechanical and thermal-mechanical treatments of 304 stainless steel enables yield strengths of over 200,000 psi to be obtained with elongations better than 10%. Electron microscopy, X-ray, and magnetic techniques show that during deformation strain induced $\gamma \rightarrow \varepsilon \rightarrow \alpha$ transformation occurs with further thermal nucleation of α achieved by aging up to 400°C. The yield strengths are linearly proportional to the volume fraction of α irrespective of the treatment used to form α. Softening occurs by aging at 500°C and above due to a decrease in % α. This may occur by renucleation of γ rather than by reversion. The amount of ε decreases as α increases by reversion $\varepsilon \rightarrow \gamma$.

The system is best described as a composite with hard martensite particles formed within the austenite. The amount of α can be controlled (and thereby the properties) by the mechanical/thermal-mechanical processing.

ACKNOWLEDGEMENTS

This work was done under the auspices of the United States Atomic Energy Commission through the Inorganic Materials Research Division of the Lawrence Radiation Laboratory. Helpful discussions with Professors E. R. Parker and M. F. Ashby are acknowledged.

REFERENCES

1. P. L. Mangonon, Jr. and G. Thomas (Part I), Trans. AIME, 1969.
2. K. H. Kayer, Draht, 1967, 18, No. 3, 121.
3. N. A. Ziegler and P. H. Brace, Proc. ASTM, 1950, 50, 861.
4. G. B. Espey, A. J. Rapko, and W. F. Brown, Proc. ASTM, 1959, 59, 816.
5. D. T. Llewellyn and J. D. Murray, Special Report No. 86, Iron and Steel Inst. (London) 1964, 197.
6. C. R. Mayne, ASTM STP No. 287, 1961, 150.
7. S. Floreen and J. R. Mihalism, ASTM STP 369, 1965, 17.
8. A. N. Chukhleb and V. P. Martynov, Phys. Metals and Metallography, 1960, 10, (2), 80.
9. V. I. Grigorkin, Physics of Metals and Metallography, 1962, 14 (2), 45.
10. J. P. Bressanelli and A. Moskowitz, Trans. ASM, 1966, 59, 223.
11. P. L. Mangonon, Jr., Ph.D. Thesis, Department of Mineral Technology, University of California, Aug. 1968, UCRL Report #18230.
12. W. J. M. Tegart, "Elements of Mechanical Metallurgy", 1966, p. 29, (The Macmillan Company, N.Y.).
13. V. F. Zackay, W. W. Gerberich, R. Busch, and E. R. Parker, UCRL Report #16363, 1965, University of California, Lawrence Radiation Laboratory, Berkeley, California.
14. K. Hoselitz, "Ferromagnetic Properties of Metals and Alloys" (Oxford Clarendon Press, Oxford, 1952).
15. B. Cina, J. Iron and Steel Inst., 1954, 177, 406.
16. C. J. Guntner and R. P. Reed, Trans. ASM, 1962, 55, 399.
17. R. P. Reed, Acta Met., 1962, 10, 865.
18. J. A. Hren and G. Thomas, Trans. AIME, 1963, 227, 308.

19. O. Johari and G. Thomas, Trans. ASM, 1965, 58, 563.

20. V. F. Zackay, E. R. Parker, D. Fahr, and R. Busch, Trans. ASM, 1967, 60, 252.

21. A. Kelly and R. B. Nicholson, Prog. Mat. Sci., 1963, 10.

22. M. von Heimendahl and G. Thomas, Trans. AIME, 1964, 230, 1520.

23. B. A. Wilcox and R. I. Jaffee, Trans. Jap. Inst. Met, 1968, 9 (Suppl), 575.

24. A. Kelly, "Strong Solids" Clarendon Press, Oxford, 1966.

25. D. L. McDanels, R. W. Jech and J. W. Weeton, Metal Prog., (1960), 78(6), 118.

26. J. W. Christian, "The Physical Properties of Martensite and Bainite", Iron and Steel Inst. (London) Special Report 93, 1965, 1.

27. G. V. Kurdgumov, et al., "Physics of Metals and Metallography", 1958, 6, (No. 1) 85.

APPENDIX

Calculation of Volume Fraction of α Phase

The amount of magnetic phase present is calculated from the measured magnetic saturation B_s and using the reported specific saturation magnetization per unit mas (σ_s) of 160.4 for 100% α martensite[22] in an alloy almost identical to the one used here. (See also Ref. 20).

Magnetic moment/unit mass $\sigma_s = B_s/4\pi\rho_\alpha$ where B_s is the intrinsic saturation magnetization and values are given in Tables II and III. ρ_α is the density of the α phase (bcc)

$1/\rho_\alpha = (1/\rho_{Fe})N_{Fe} + (1/\rho_{Cr})N_{Cr} + (1/\rho_{Ni})N_{Ni}$, etc., where Ni is weight fraction of i^{th} component thus

$$\frac{1}{\rho_\alpha} = \left(\frac{1}{7.87}\right) 0.74 + \left(\frac{1}{7.19}\right) 0.18 + \left(\frac{1}{8.90}\right) 0.08$$

From which $\rho_\alpha = 7.77$ gm/cm^3. The volume fraction of α is thus

$$C\alpha = \frac{\sigma_s}{160.4}$$

The values obtained by this method were checked against values obtained on the same sample by X-ray intensity measurements, and the agreement was excellent. Thus, the magnetic technique was utilized to obtain the volume fractions of α, which are given in Fig. 13 and Table II.

Table I. Tabulated room temperature mechanical properties.

% Tensile Strain at LN	Aging Temp, °C	Yield Strength (0.1% offset), psi	Tensile Strength psi	% Elongation in 2"
3.5%	R.T.	75,800	131,000	42.0
3.5%	200°C	63,400	116,000	43.0
3.5%	300°C	67,900	116,700	43.5
4.5%	400°C	71,500	119,800	39.0
4.5%	500°C	66,200	115,500	42.0
10%	R.T.	95,000	156,500	7.5†
10%	100°C	103,500	153,500	9.0†
9.5%	200°C	82,600	130,000	5.0†
8.5%	300°C	96,800	136,700	10.5†
9.5%	400°C	98,200	136,700	5.0†
10%	500°C	93,200	134,000	14.5†
16%	R.T.	141,000	184,000	15.5
15%	100°C	147,200	186,000	15.2
15%	200°C	165,000	183,500	17.5
15%	300°C	161,000	182,000	17.0
15%	400°C	154,000	188,500	18.0
15%	500°C	128,000	154,500	25.5
19.75%	R.T.	177,000	195,000	4.5†
19.5 %	100°C	176,000	182,000	2.0†
20.0 %	200°C	197,000	198,000	11.8
19.5 %	300°C	199,000	201,000	11.0
20.25%	400°C	217,000	219,000	2.0†
20%	500°C	155,000	169,500	18.5†
25.25%	R.T.	215,000	*	∿0%†
24.0 %	400°C	244,000	*	∿0.5%†

† Specimen broke outside of gage marks.

* Catastrophic failure

Table II. Effect of further thermomechanical treatment.

(Deformation by rolling)

Sample	Thermomechanical Treatment	B_s,(gauss) Saturation Magnetization (% α')	Yield Strength 0.1% offset psi	Tensile Strength psi	% Elongation in 2"
A1	Rolled,20% reduction in thickness at LN	9.920 (63%)	187,000	199,000	9%
A21	Same as A1, then aged at 400°C for 2 hrs.	10,550 (67%)	216,000	*	5%
A22	Same as A1, then rolled at 400°C 9% reduction in thickness	10,790 (68.5%)	231,000	234,000	1%
A31	Same as A21, then rolled at R.T. 9% reduction in thickness	11,090 (70.5%)	219,000	225,000	5%
A32	Same as A31, then aged at 400°C for 2 hrs.	11,100 (70.6%)	242,000	*	1%
A41	Same as A21 rolled at LN, 9% reduction in thickness	10,940 (69.7%)	216,000	224,000	5%
A42	Same as A41, then aged at 400°C for 2 hrs.	11,600 (73.7%)	255,000	*	1%

* Catastrophic failure

Table III. Tabulated results of magnetic measurements.

% Tensile Strain at LN	B_s, saturation magnetization gauss		Aging Temperature °C	ΔB_s gauss After Aging
	before aging	after aging		
0%	0	0	----	----
3.5%	580	---	R.T.	----
3.5%	580	567	200°C	- 13
3.5%	627	587	300°C	- 40
4.5%	780	772	400°C	- 8
4.5%	920	613	500°C	-307
10%	4.180	---	R.T.	----
10%	3,555	3,605	100°C	- 50
9.5%	3,240	3,290	200°C	- 50
8.5%	2,955	3,055	300°C	+ 70
9.5%	3,220	3,325	400°C	+105
10%	3,370	2,630	500°C	-740
16%	6,570	---	R.T.	----
15%	6,830	6,870	100°C	+ 40
15%	7,180	7,210	200°C	+ 30
15%	6,980	7,110	300°C	+130
15%	6,810	7,080	400°C	+270
15%	5,010	4,350	500°C	-1660
19.75%	8.490	---	R.T.	----
19.5%	7,800	7,770	100°C	- 30
20%	8,340	8,340	200°C	0
19.5%	8,390	8,560	300°C	+170
20.25%	8,820	9,280	400°C	+460
20%	8,740	6,400	500°C	-2340
25.25%	10,300	---	R.T.	----
24%	10,250	10,680	400°C	+430

FIGURE CAPTIONS

Fig. 1 - Yield strenths of 304 steels at room temperature after aging 1 1/2 hours at the temperatures shown following tensile deformation at -196°C. These property changes are related to % α.

Fig. 2 - As Fig. 1 showing ultimate tensile strengths.

Fig. 3 - As Fig. 1 showing % elongation.

Fig. 4 - Variation in the saturation magnetization at room temperature after tensile deformation in liquid nitrogen.

Fig. 5 - Changes in saturation magnetization after the thermal-mechanical treatments indicated.

Fig. 6 - X-ray diffractometer traces of 304 steel at room temperature following 10% deformation in liquid nitrogen; a) as deformed; b) aged 1 1/2 hrs at 200°C; c) aged 1 1/2 hrs at 400°C.

Fig. 7 - Showing the variation in volume fraction of γ, ε and α phases at room temperature after tensile deformation in liquid nitrogen.

Fig. 8 - X-ray diffractometer traces of the 200 α reflection at room temperature after 10% reduction in thickness in liquid nitrogen.

Fig. 9 - Specimen deformed 15% at -196°C and aged at room temperature. The α particles have grown into the γ phase and ε reverts to γ. Notice alignment of α laths in one direction.

Fig. 10 - Specimens deformed 15% at -196°C showing blocky α particles (strain induced) at A containing carbides (circled); thermally nucleated α at N. Reversion of ε → γ has occurred at S. a)bright field; b) dark field of α reflection; c) dark field of α (strain induced) and d) dark field of α (thermal). Notice that the α phases in c and d differ in orientation.

Fig. 11 - Contrast experiments to show thermally nucleated α marked 2 has a different orientation from stress induced α as seen by the contrast reversals in the dark field images of α(2) in (b) α 1 in (c). (a) is the bright field; d is a dark-field image using a γ reflection. (e.g., to Fig. 10). Specimens deformed 15% at -196°C then aged 1 1/2 hrs 200°C.

Fig. 12 - Microstructure of 304 steel after 10% strain at -196°C followed by 1 1/2 hrs aging at 500°C; a) bright field; b) dark field using only γ reflection. Notice γ regions F within α phase A.

Fig. 13 - Summary of results showing the yield strength is linearly determined by the % α irrespective of the manner or amount of thermal-mechanical/mechanical treatment.

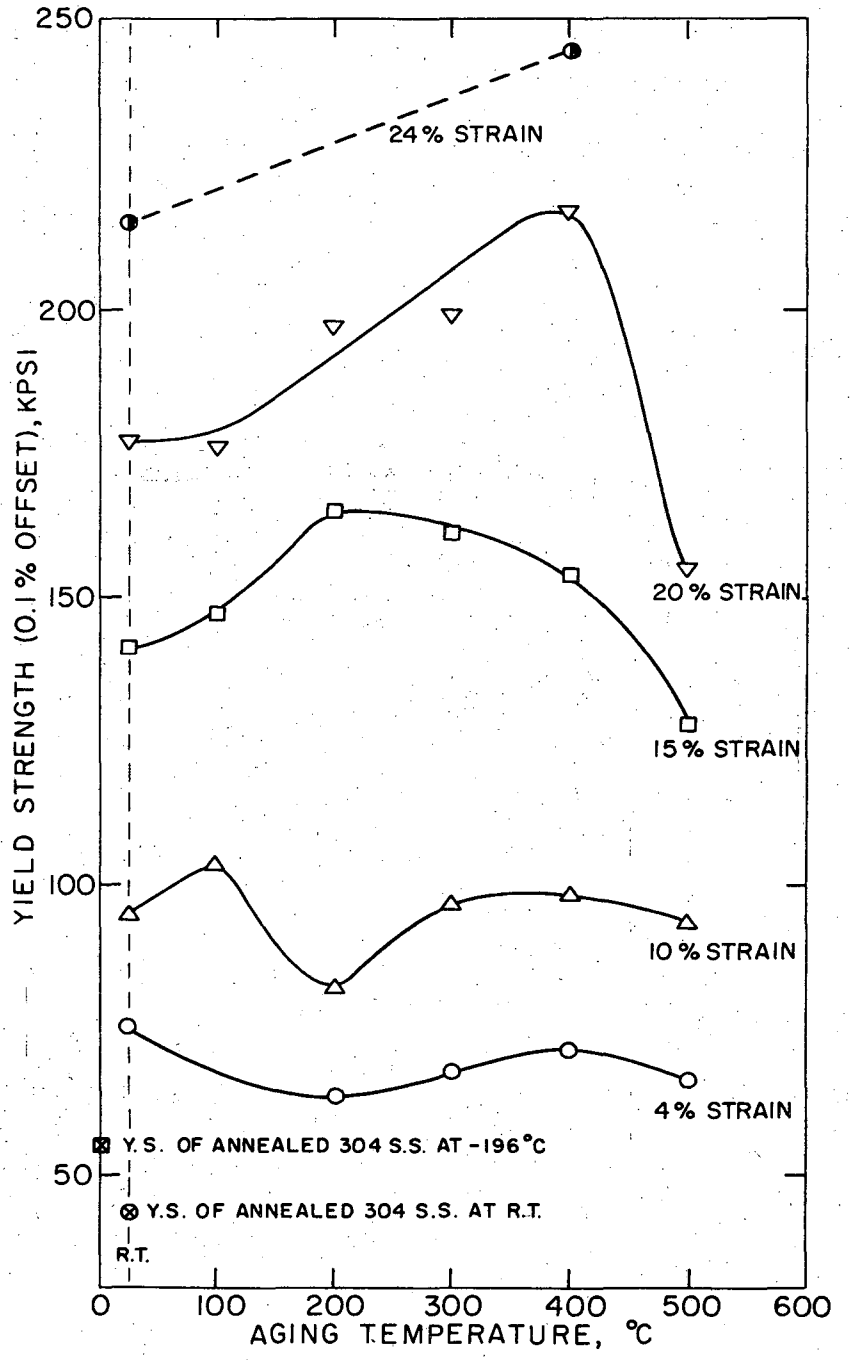

XBL 687-1284

Fig. 1

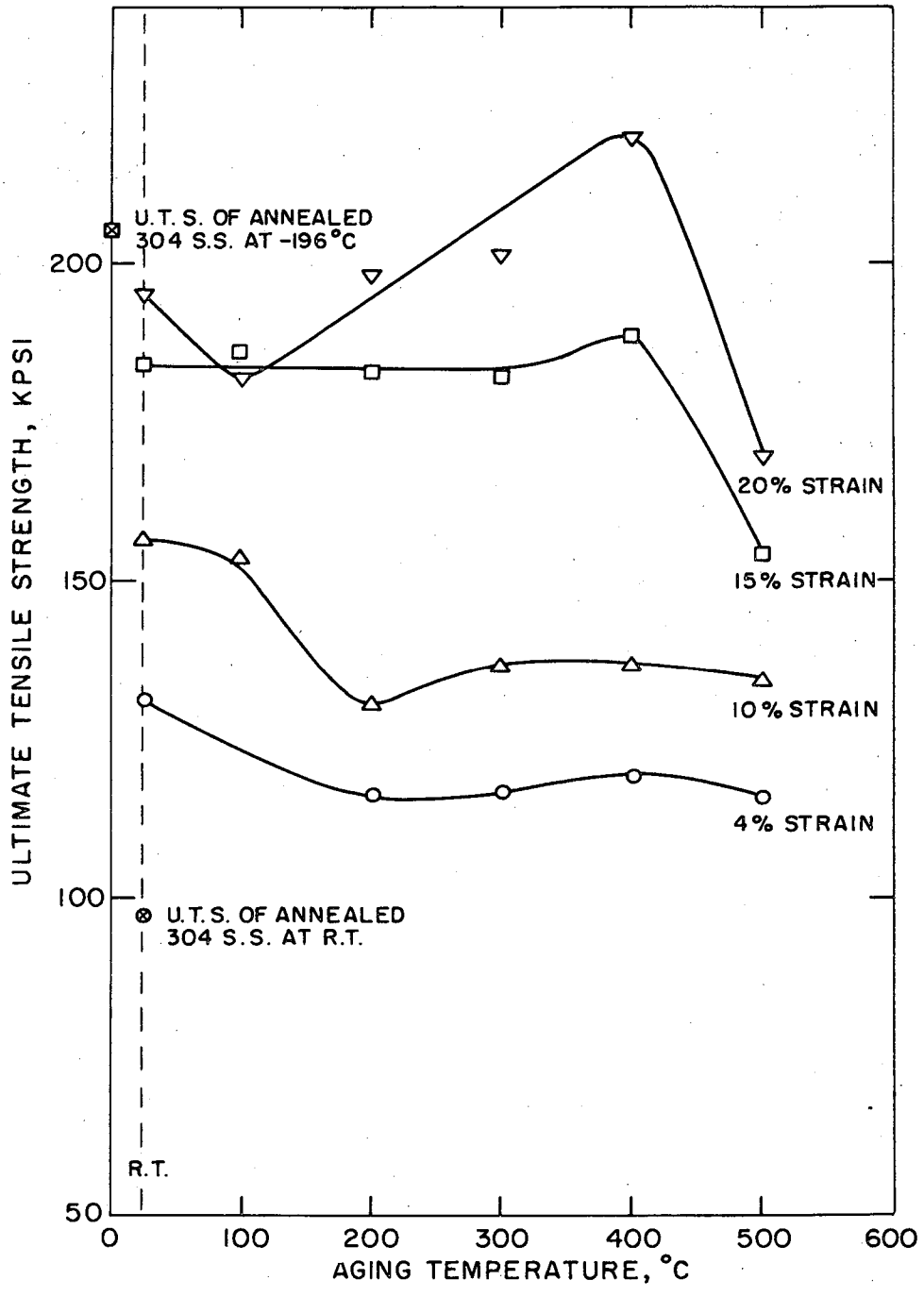

XBL 687-1285

Fig. 2

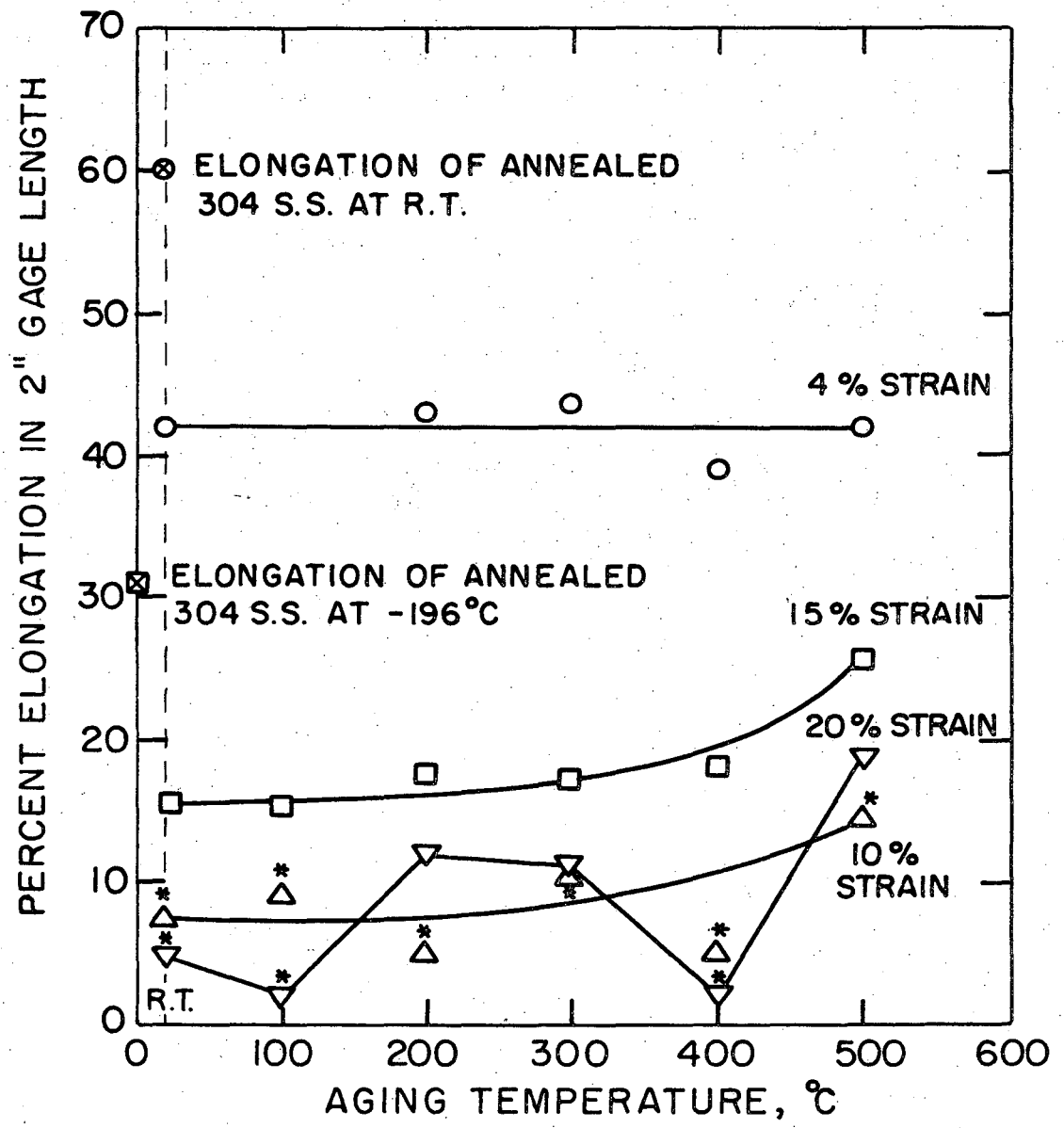

XBL 687-1286

Fig. 3

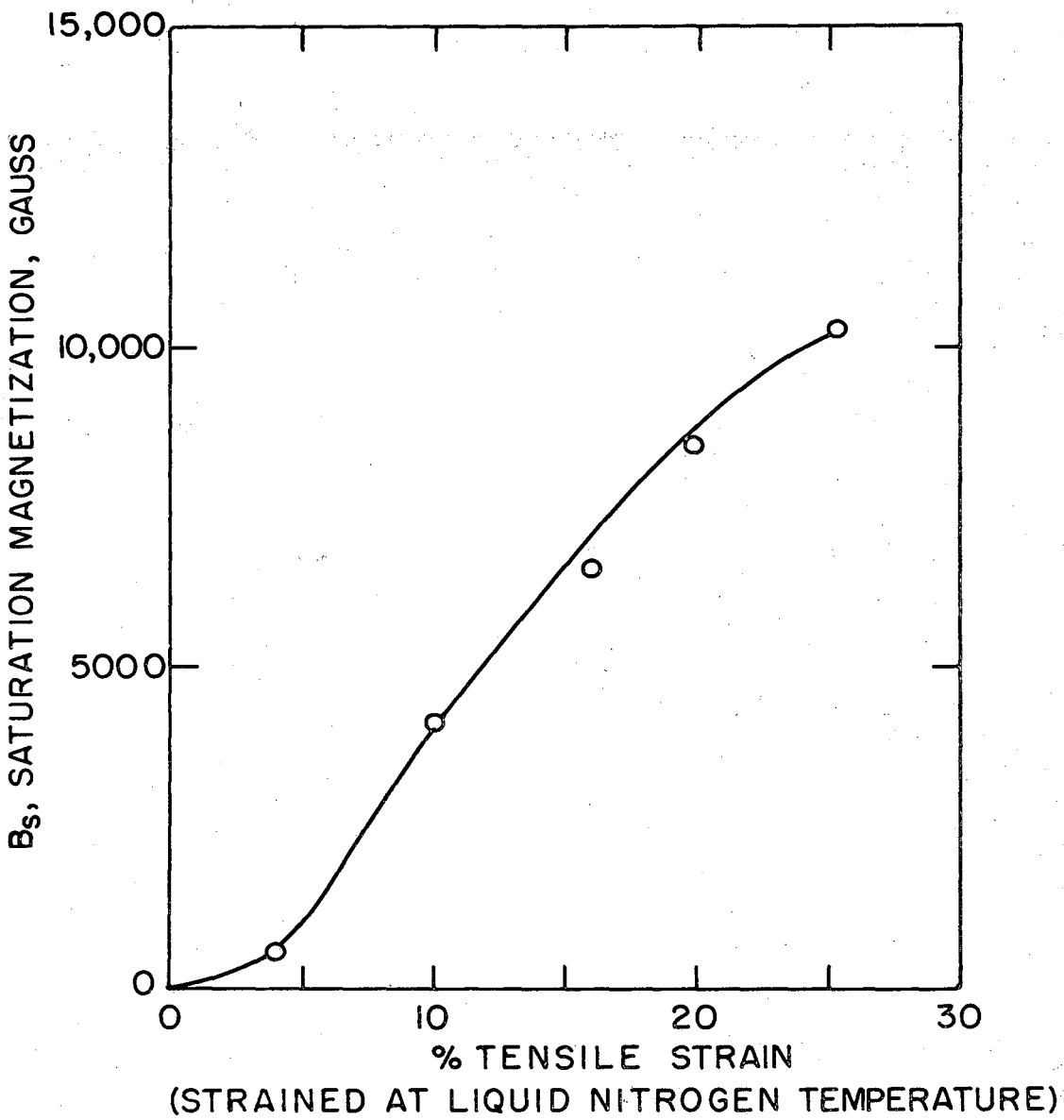

XBL 687-1281

Fig. 4

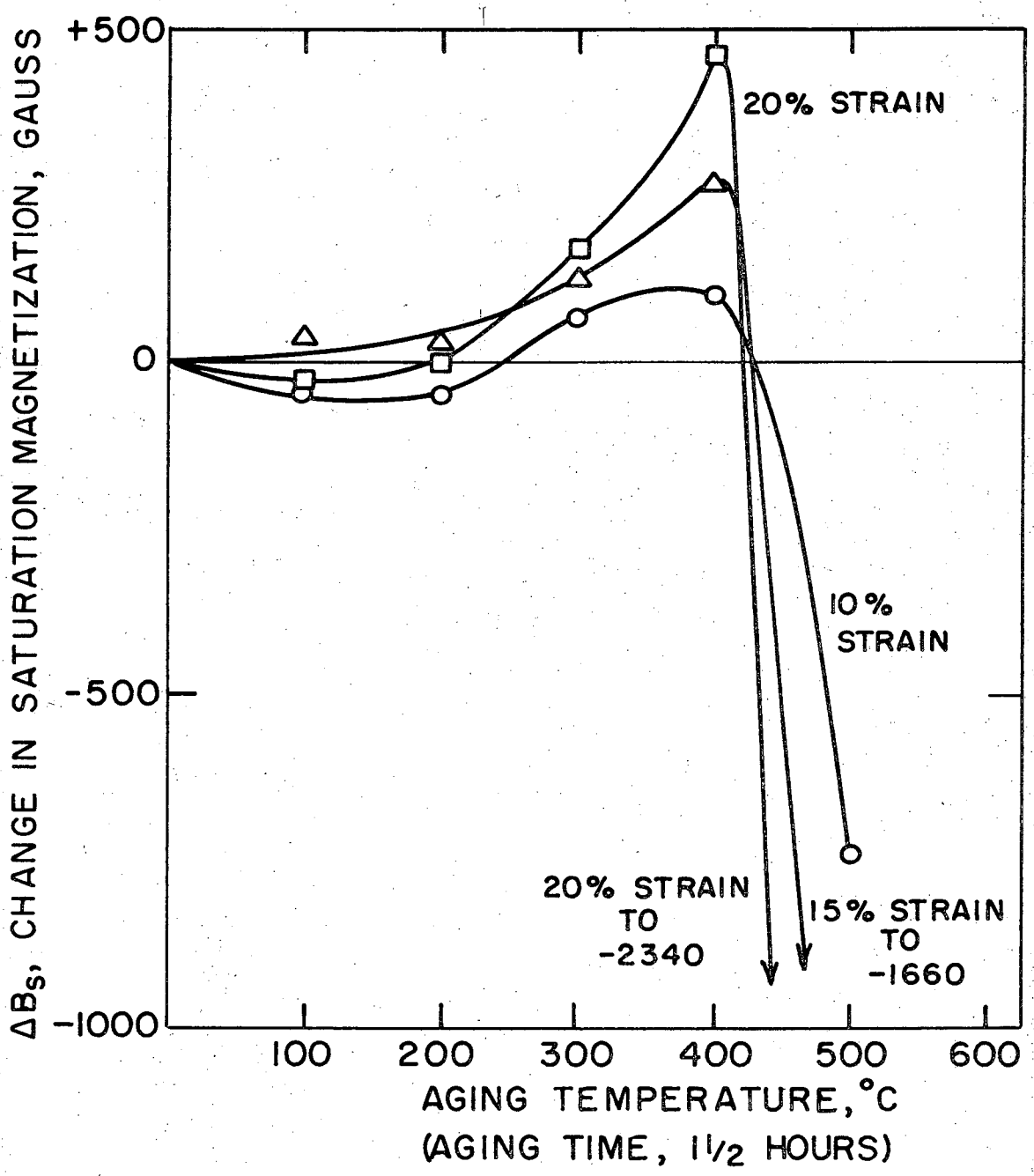

XBL 687-1282

Fig. 5

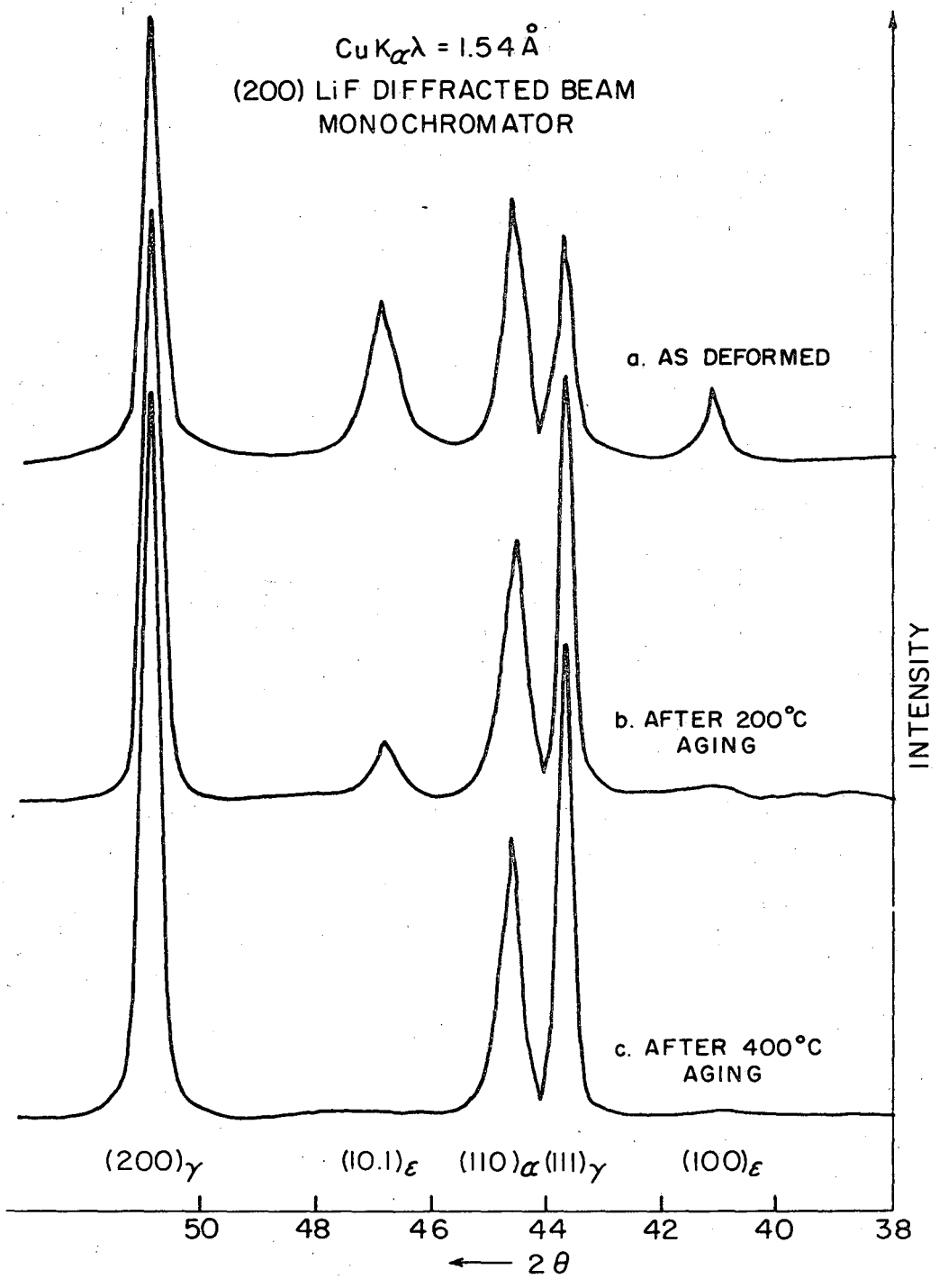

XBL 687-1287

Fig. 6

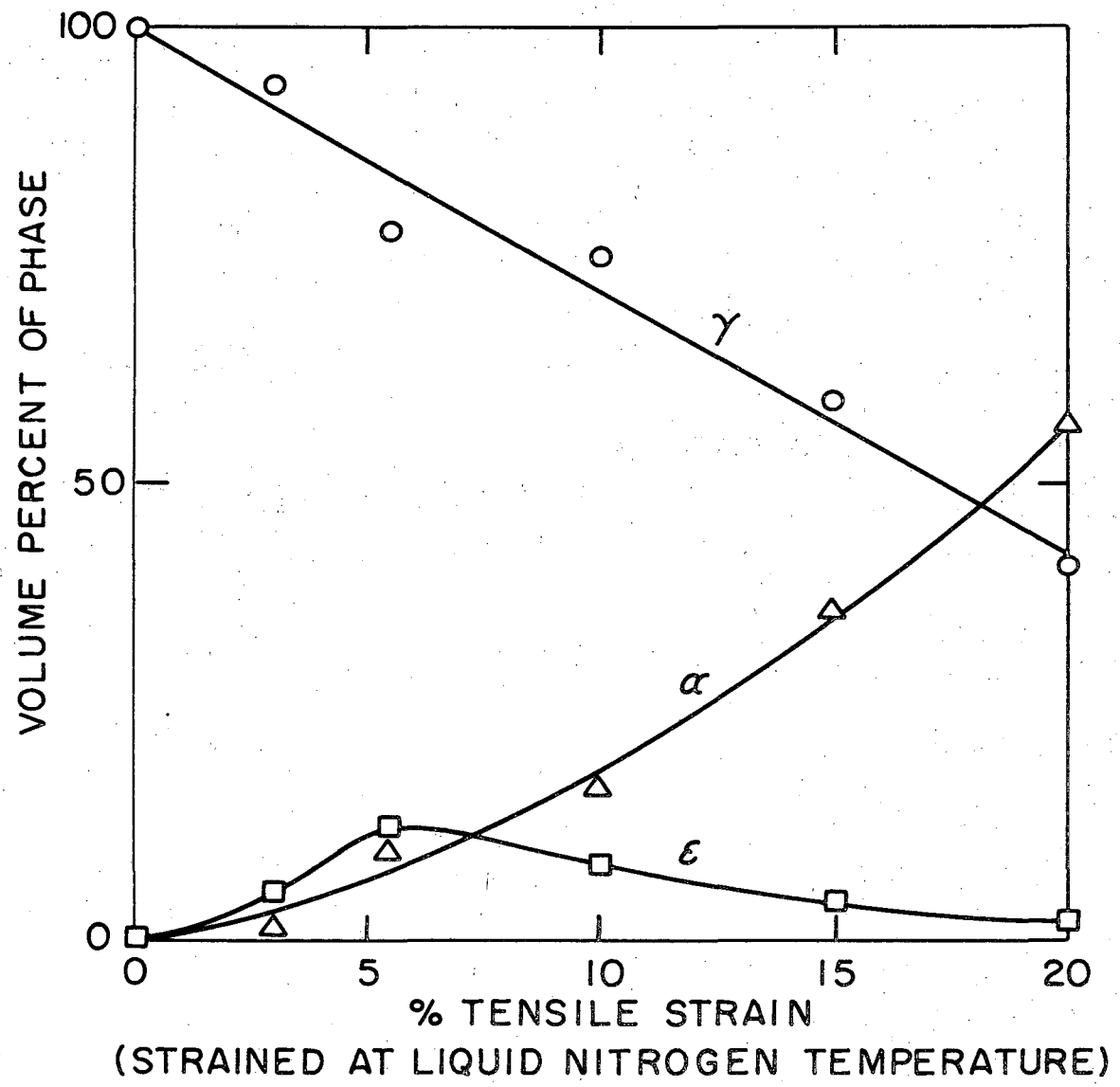

XBL 687-1288

Fig. 7

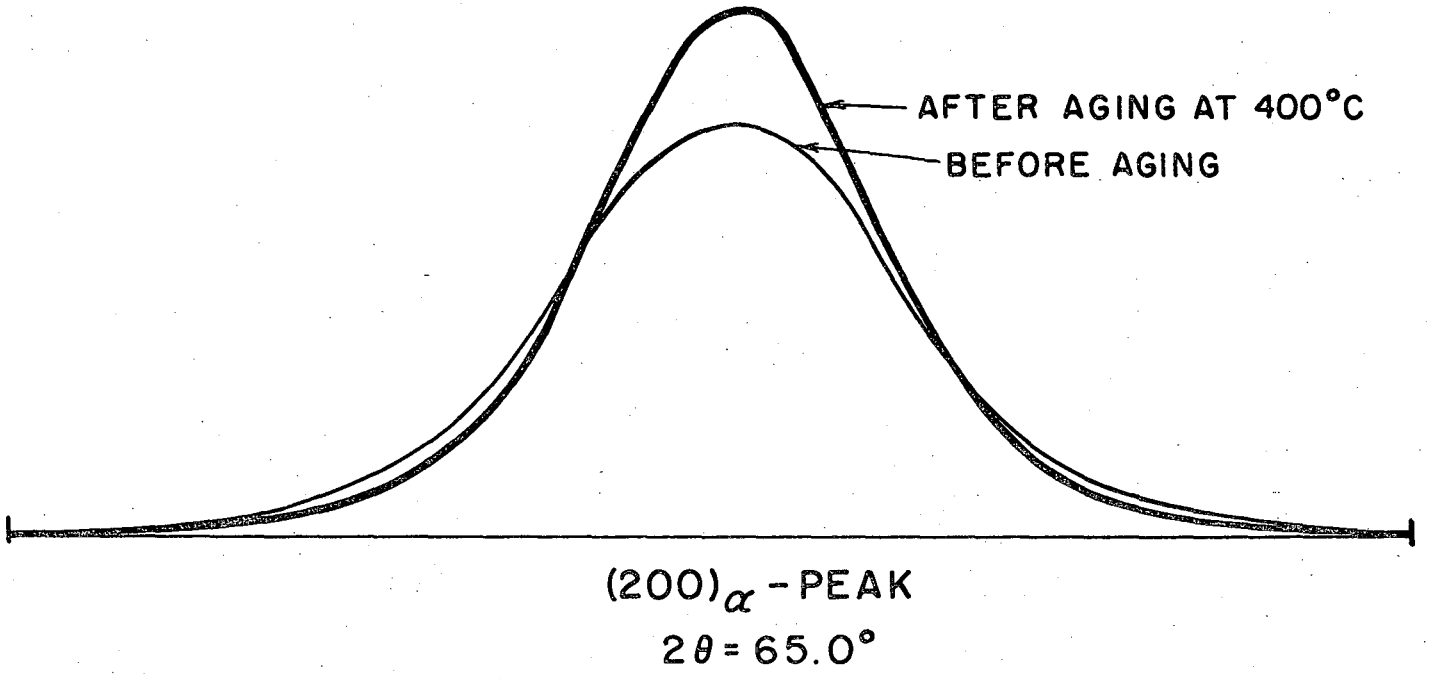

XBL 687-1298

Fig. 8

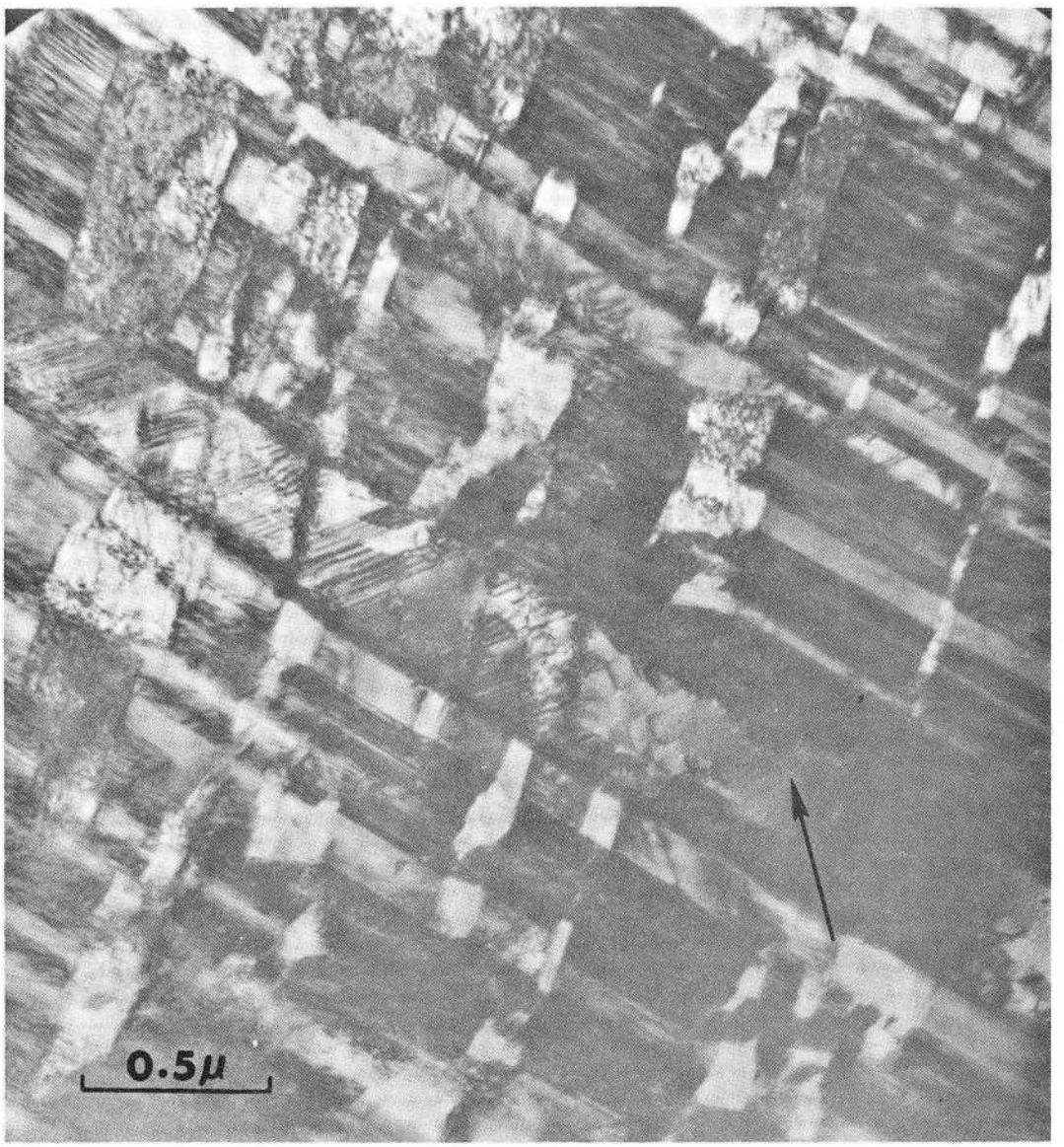

XBB 685-2528

Fig. 9

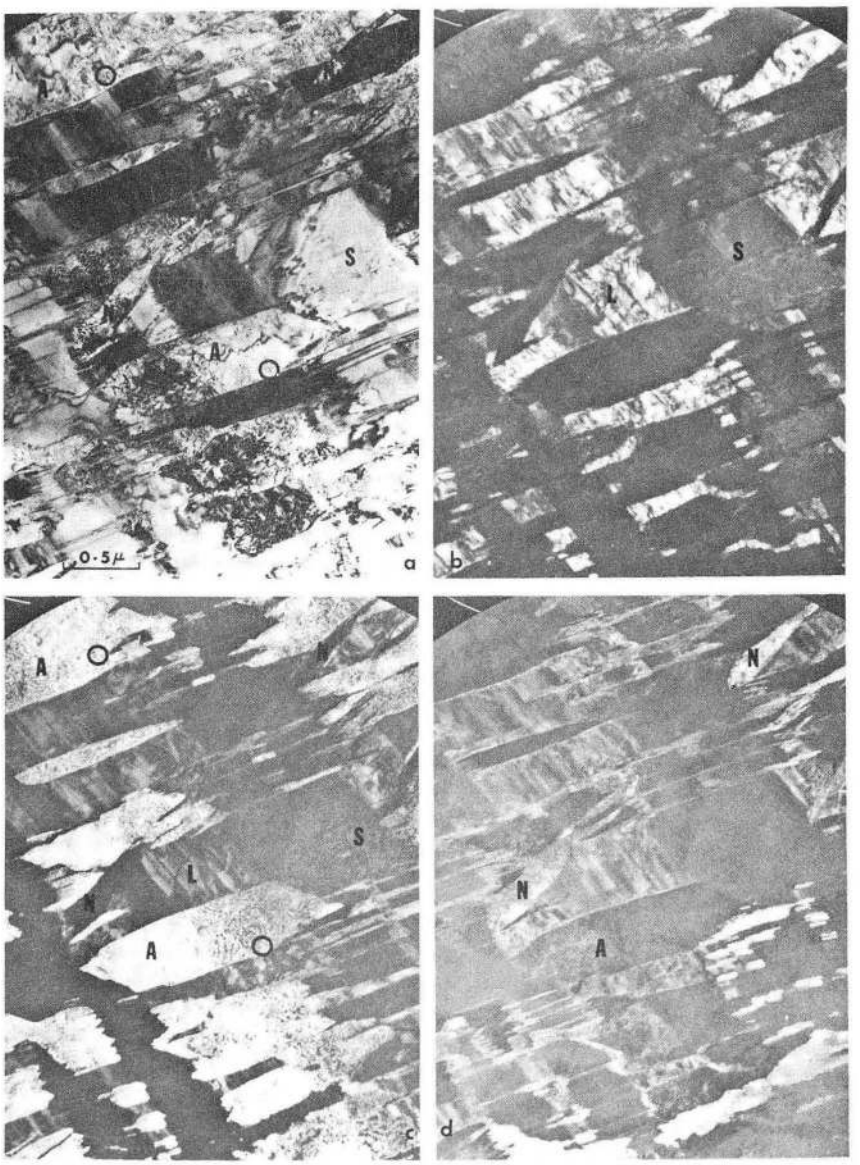

XBB 687-4086-A

Fig. 10

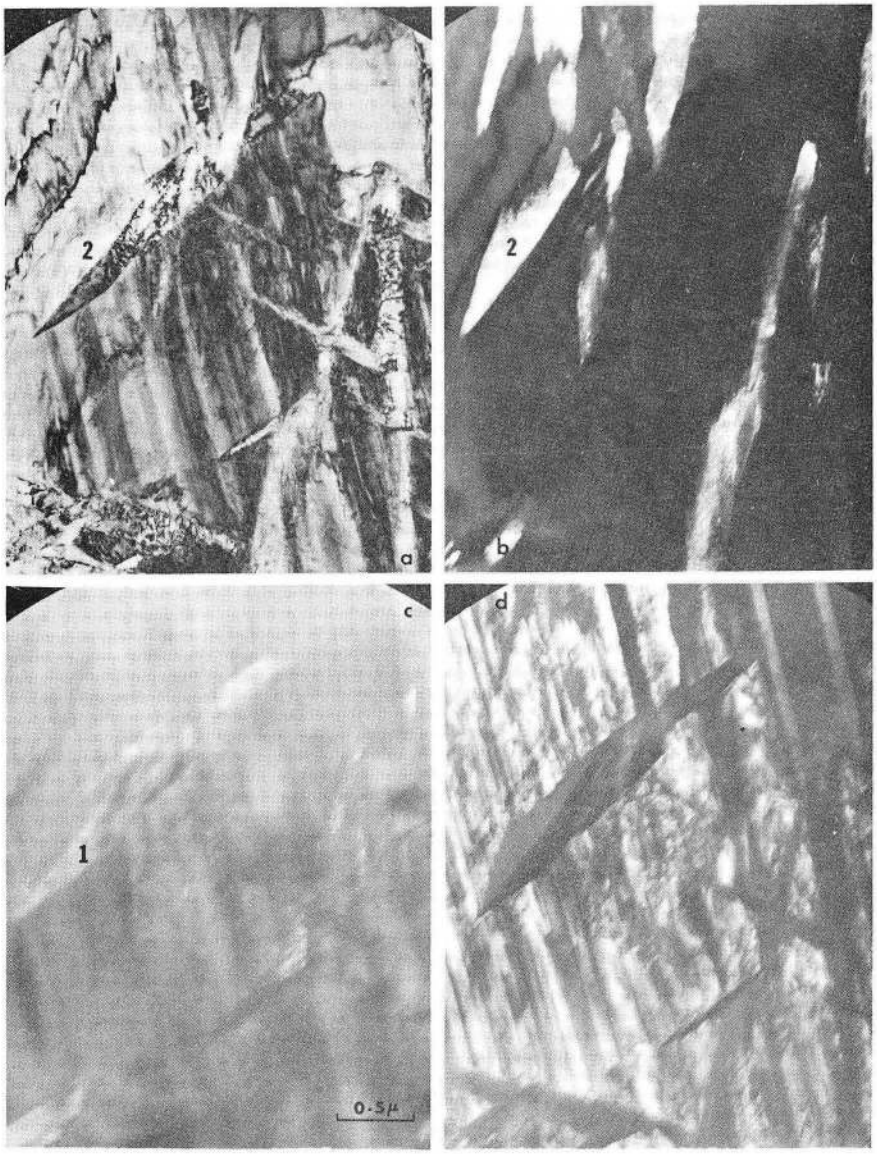

XBB 687-4087-A

Fig. 11

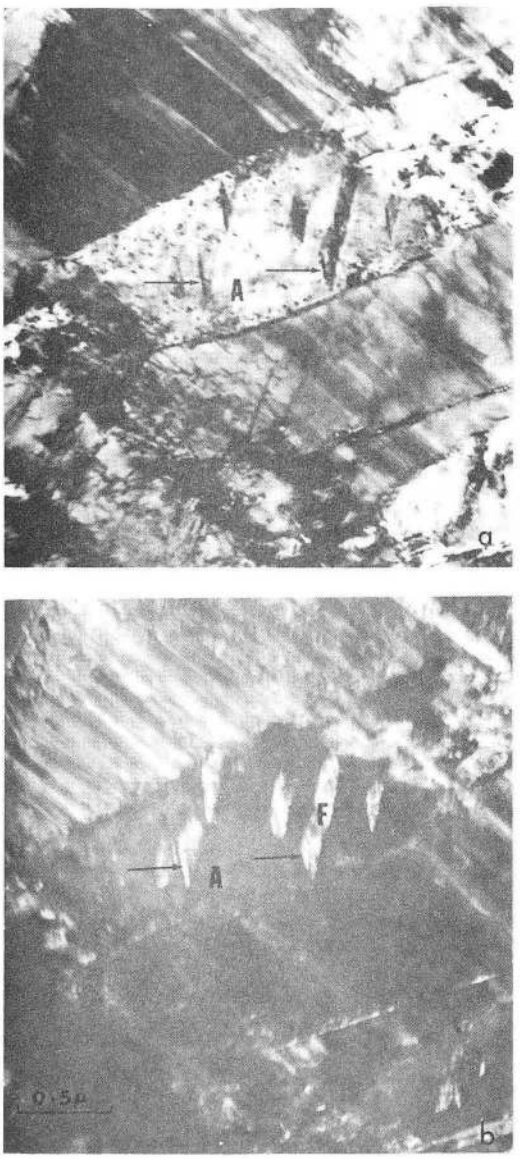

XBB 687-4090-A

Fig. 12

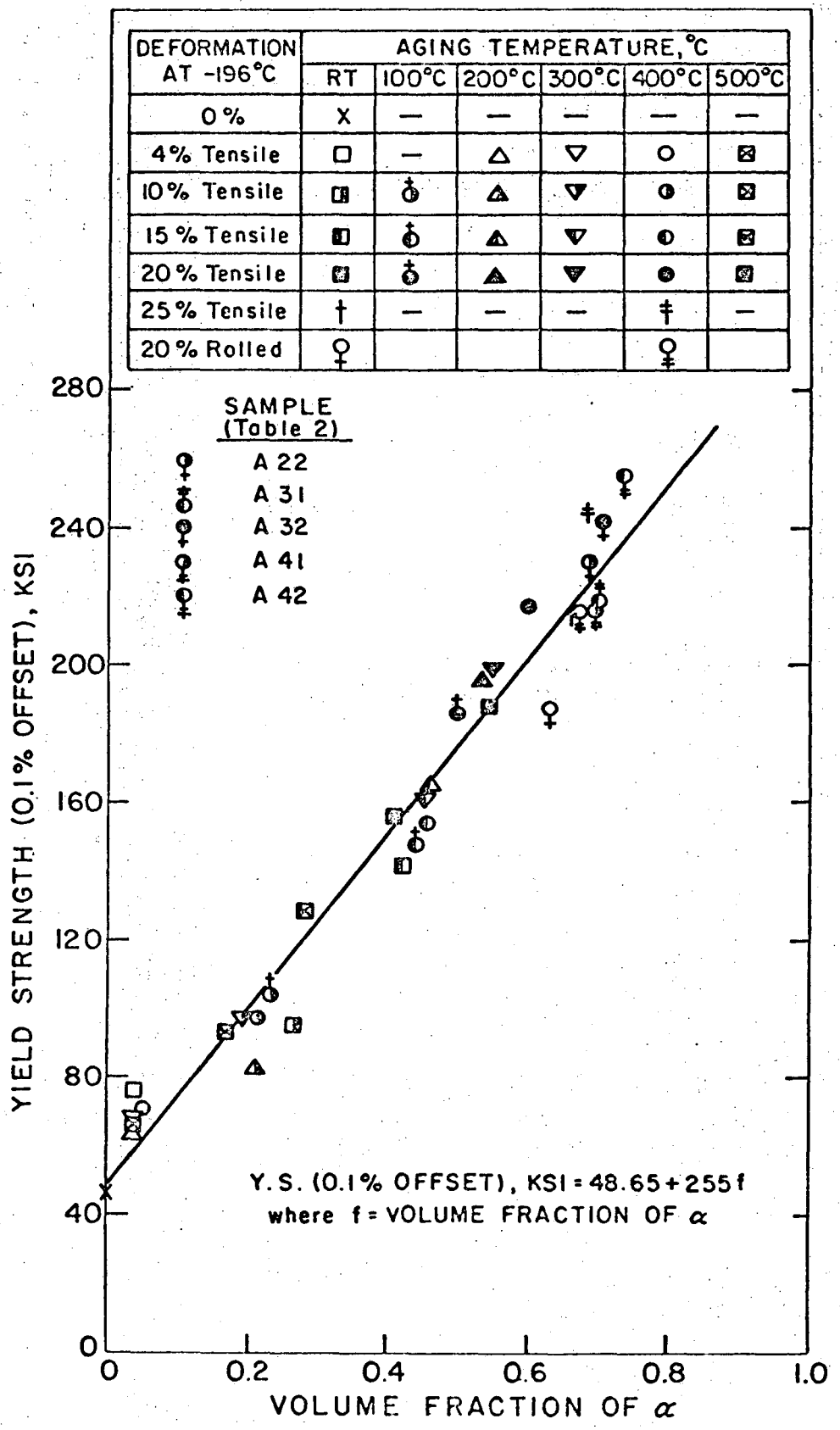

XBL 696-650

Fig. 13

LEGAL NOTICE

TECHNICAL INFORMATION DIVISION
LAWRENCE RADIATION LABORATORY
UNIVERSITY OF CALIFORNIA
BERKELEY, CALIFORNIA 94720